Shock Waves in Polycrystalline Iron

Kai Kadau,[1,*] Timothy C. Germann,[2,†] Peter S. Lomdahl,[1,‡] Robert C. Albers,[1,§] Justin S. Wark,[3,‖] Andrew Higginbotham,[3,¶] and Brad Lee Holian[2,**]

[1]*Theoretical Division, Los Alamos National Laboratory, Los Alamos, New Mexico 87545, USA*
[2]*Applied Physics Division, Los Alamos National Laboratory, Los Alamos, New Mexico 87545, USA*
[3]*Department of Physics, Clarendon Laboratory, University of Oxford, Oxford OX1 3PU, United Kingdom*
(Received 18 October 2006; published 26 March 2007)

The propagation of shock waves through polycrystalline iron is explored by large-scale atomistic simulations. For large enough shock strengths the passage of the wave causes the body-centered-cubic phase to transform into a close-packed phase with most structure being isotropic hexagonal-close-packed (hcp) and, depending on shock strength and grain orientation, some fraction of face-centered-cubic (fcc) structure. The simulated shock Hugoniot is compared to experiments. By calculating the extended x-ray absorption fine structure (EXAFS) directly from the atomic configurations, a comparison to experimental EXAFS measurements of nanosecond-laser shocks shows that the experimental data is consistent with such a phase transformation. However, the atomistically simulated EXAFS spectra also show that an experimental distinction between the hcp or fcc phase is not possible based on the spectra alone.

DOI: 10.1103/PhysRevLett.98.135701 PACS numbers: 64.70.Kb, 62.50.+p, 64.70.Nd, 71.15.Pd

Because of its technological, geological, and sociological importance, iron is one of the most studied materials. In particular, phase changes—due to pressure or temperature—from the ferromagnetic body-centered cubic (bcc) ground state into nonferromagnetic close-packed structures—and vice-versa—are of interest, since they are the origin for many important properties of iron. Based on wave-profile analysis, in 1956 D. Bancroft *et al.* [1] discussed the possibility of a structural phase transformation in iron under shock loading above 13 GPa. In 1962 Jamieson [2] found that bcc iron transforms under static pressure into the hexagonal-closed packed (hcp) structure. Ever since, it was assumed that the same transition occurred under dynamic shock loading. In 2002, by large-scale molecular-dynamics (MD) simulations of shock propagation along the $[001]_{\mathrm{bcc}}$ direction in iron single crystals, the transformation into the hcp structure was observed [3]. Three years later, ultrafast *in situ* x-ray diffraction of shocks traveling in the $[001]_{\mathrm{bcc}}$ direction not only confirmed the earlier theoretical prediction, but also constituted the first experimental proof for the shock-induced bcc $\rightarrow$ hcp transition [4]. However, it still has not been conclusively demonstrated that the shock-induced product structure is hcp for shocks along other single-crystal directions, or for polycrystalline iron. In fact, recent MD simulations have discussed the possibility that the product phase consists partly of a metastable face-centered cubic (fcc) structure that may be kinetically favored for shocks along other directions [5]. Yaakobi *et al.* [6] analyzed *in situ* extended x-ray absorption fine structure (EXAFS) of nanosecond-laser-generated shock waves in 8 μm thick polycrystalline iron samples. The EXAFS data showed a phase transformation from the bcc into a close-packed structure, which the authors identified as hcp.

Here, we present large-scale nonequilibrium MD (NEMD) simulations of shock waves in polycrystalline iron in order to compare to experimental data. In particular, the EXAFS spectra are calculated from the atomic configurations obtained by simulations and compared to the experimental data sets. Samples containing about 30×10^6 atoms were simulated using our scalable parallel short-range molecular-dynamics (SPASM) code . The interatomic forces were described by the embedded-atom method (EAM) [10–12] as has been used in previous studies for shock waves in iron single crystals [3,5]. This potential yields cold curve transition pressures of 9.0 GPa (bcc $\rightarrow$ hcp) and 13.5 GPa (bcc $\rightarrow$ fcc), which compares to 11.5 and 19 GPa as obtained by *ab initio* calculations, respectively [5,13]. Polycrystalline samples were obtained by picking at random 32–1024 grain centers and orientations and filling the space with the crystallographic orientation according to the nearest grain center. This results in a Poisson-Voronoi lattice for which the mean grain size can be defined as the mean caliper diameter $d = 1.458n^{-1/3}$ (n = grain center density) [14]. The samples, with grain sizes between 10.3 and 32.7 nm, were then equilibrated for 1.46 ps at about 500 K followed by a kinetic annealing procedure for another 1.46 ps in order to minimize the potential energy of the grain boundaries. Longer annealing times or higher equilibration temperatures did not change significantly the structure of the grain boundaries nor the response of the samples under shock loading. Once the polycrystalline sample is prepared, random atomic velocities are assigned to yield the desired initial temperature (50 or 300 K). A shock wave with particle velocity u_p is generated by the momentum mirror method, whereby the sample is slammed up against a specularly reflecting wall [15]—no temperature or pressure control is applied, since a nonequilibrium phenomenon is simulated. More than 30 different simulations were performed for the present study.

Upon the passage of a shock wave, the polycrystal reacts differently depending on the shock strength [16], but is

relatively insensitive to changes in the initial temperature (Fig. 1). For weak shock strengths up to about 10 GPa ($u_p = 0.027$ km/s), the shock wave compresses the polycrystal only elastically. No evidence of bcc plasticity (such as dislocations) is detected, which might be attributed to the short time scales accessed in the simulations (several picoseconds) and in laser-generated shocks (some nanoseconds) [4], where bcc plasticity is also absent. Experimentally, on longer time scales bcc plasticity seems to be present [17,18]. Larger pressures start to plastically deform the crystal by nucleating a close-packed structure (mainly hcp) at grain boundaries. Here, the dominant wave is still the elastic wave, since the transformation takes place slowly near grain boundaries and also grows in all directions, not only the direction of the shock. For pressures of 20 GPa ($u_p = 0.54$ km/s) and above, a two-wave structure is observed, which becomes a single overdriven transformation wave above about 50 GPa ($u_p = 1.09$ km/s). To within noise no difference in the observed transformation mechanism or the Hugoniot data was observed with varying grain size.

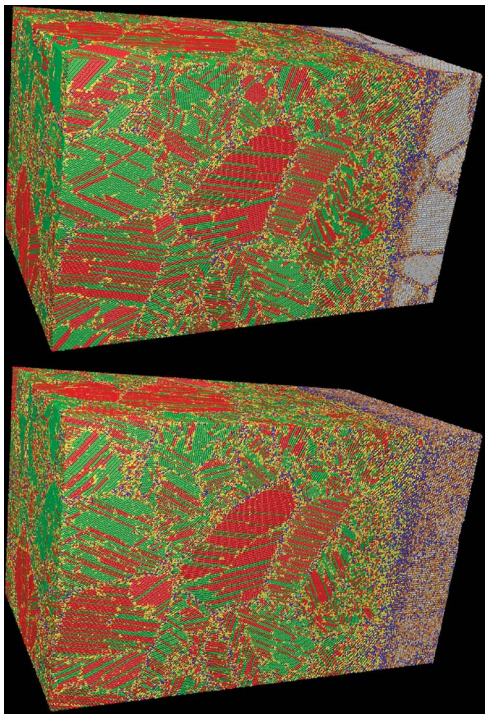

FIG. 1 (color). Samples shocked with $u_p = 0.906$ km/s, 14.6 ps after the impact. Top (bottom) sample has an initial temperature of 50 K (300 K) and reaches a temperature behind the shock front of 296 K (622 K), pressures of about 39 GPa, and volume compressions of 19%. The samples consist of 32 grains and about 30 M atoms confined in a 57.4 nm × 57.4 nm × 109.9 nm box. Color coding denotes the local neighborhood of each atom: gray: bcc, blue: uniaxially compressed bcc, yellow: grain-boundary, red: hcp, green: fcc (see [5] for details). Fluctuations in the bcc structure at 300 K (bottom) wash out the color scheme analysis, and therefore make it hard to see the grain-boundary structure between the bcc grains. The hcp/fcc ratio behind the shock front is on average 1.5 for this shock strength and increases with decreasing shock strength. The initial average grain-size—as defined by the average caliper diameter—is 32.7 nm.

The polycrystalline Hugoniot (i.e., the locus of final shock states), as given by the u_s-u_p (u_s = shock velocity) or the pressure-volume representation, compares reasonably well to the experimental data set [19,20]—even more so when taking into account that the EAM potential [12] was not fitted to shock or any other high-pressure data (Fig. 2). One difference to the single-crystal Hugoniot [5] are the elastic branches in the split-two-wave region. The polycrystalline microstructure not only averages over the various elastic branches, but also allows for quicker nucleation at grain boundaries compared to the single crystalline case. The somewhat higher lying (and curved) transformation wave velocities for single crystalline high symmetry directions, might be an effect of locking in a stiff microstructure that cannot relax during the observation time. These curved plastic branches for high symmetry directions have also been observed in fcc materials [21]. Eventually the single and polycrystalline Hugoniot functions converge at about $u_p = 2$–3 km/s. Because of the variation of shock velocities with crystal orientation and effects like grain-boundary scattering, the shock front has a finite width which increases in time [22,23].

The local structure around each atom can be characterized by measuring the coordination number [3], and close-packed structures (coordination 12) further identified using a centrosymmetry order parameter [5,24]. Remarkably, the hcp/fcc ratio of the product phase decreases from about 4 to 1 with increasing the shock strengths (from $u_p = 0.54$ km/s to $u_p = 1.09$ km/s). Also, the hcp/fcc ratio within a grain decreases the more the shock direction

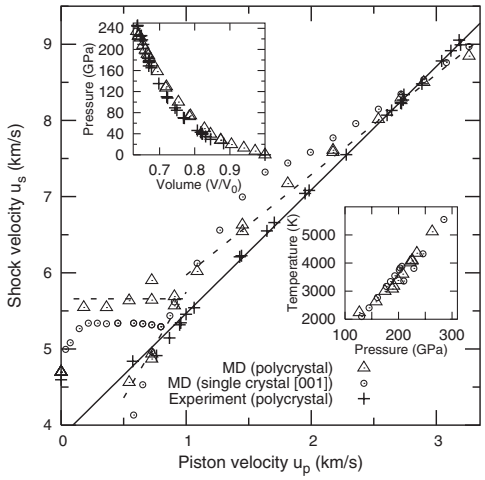

FIG. 2. Experimental and simulated Hugoniots for polycrystalline iron. The full line is a linear fit to the experimental data [19,20], the dashed lines are fits to the three different parts of the simulated Hugoniots: elastic precursor, transformation wave, and the overdriven part. As a reference, the $[001]_{bcc}$ single crystalline shock data are included [5].

deviates from the $[001]_{bcc}$ direction of the initial polycrystal. The melting transformation is probably at a similar shock strength as for single crystalline samples [5]. However, due to spontaneous premelting (or amorphization) near the shock front, with relaxation times for transforming back into the solid state depending on the distance to the real shock-induced melting, the shock-induced melting pressure could not be quantified with the relatively short samples used in this study (Fig. 2). To investigate this interesting effect, longer samples, as well as a systematic grain-size dependence, should be studied.

Yaakobi *et al.* [6] discussed one shock strength, namely, a pressure of 36 GPa, a volume compression of 20%, and a temperature rise from 300 to 645 K. Therefore, our main focus will be on a simulation that started at 300 K and was shocked with $u_p = 0.906$ km/s (Fig. 1, bottom). This resulted in a shocked state which is very close to the experimental one: 622 K, 39 GPa, and a volume compression of 19%. To analyze the structure behind the shock front and compare to experimental structure analysis, the EXAFS signal from subsets of the simulation cell has been calculated by the FEFF8 *ab initio* EXAFS software package [25]. Configurational averaging was applied to several spherical cutouts of simulation snapshots containing about 5000 atoms. This was done for several regions behind the shock front, as well as for perfect bcc, hcp, and fcc structures. For comparison, the radial distribution functions $g(r)$ were also calculated (Fig. 3). The main characteristics in the experimental data, namely, the vanishing of the peak in bcc EXAFS signal near $k = 4.25$ Å, is also clearly visible in the simulation data. The comparison between the ideal hcp and fcc signal reveals that there are only subtle differences between the two close-packed structures showing up at larger photoelectron wave numbers. Some of those differences can be seen in the simulated EXAFS and $g(r)$ curves when comparing two regions that have mainly hcp and fcc structure after the shock wave has passed. However, the experimental data are unlikely to reflect those minor difference between hcp and fcc, since the signal collection time for *in situ* shock-loading experiments is only on the order of hundreds of picoseconds. Post-recovery analysis of experimental samples is of limited use, since a reverse transformation upon reflection at the free surface takes place, as can be observed in the present simulations [16].

Comparing the ideal hcp and fcc ($P = 39$ GPa, $T = 622$ K) EXAFS and radial distribution data with the data obtained from small regions of the NEMD simulation cells, reveals that the peak positions and heights are close to each other. This demonstrates that in the simulations the product phase is indeed almost isotropic hcp ($c/a = 1.658$) and fcc (see [16] for details on c/a ratio analysis). Since the MD simulations create a classical population of phonons as compared to the correct Bose-Einstein distribution, care must be taken when comparing simulation results with experimental data below the Debye temperature—around 450 K for iron. This might be the reason why the simulated

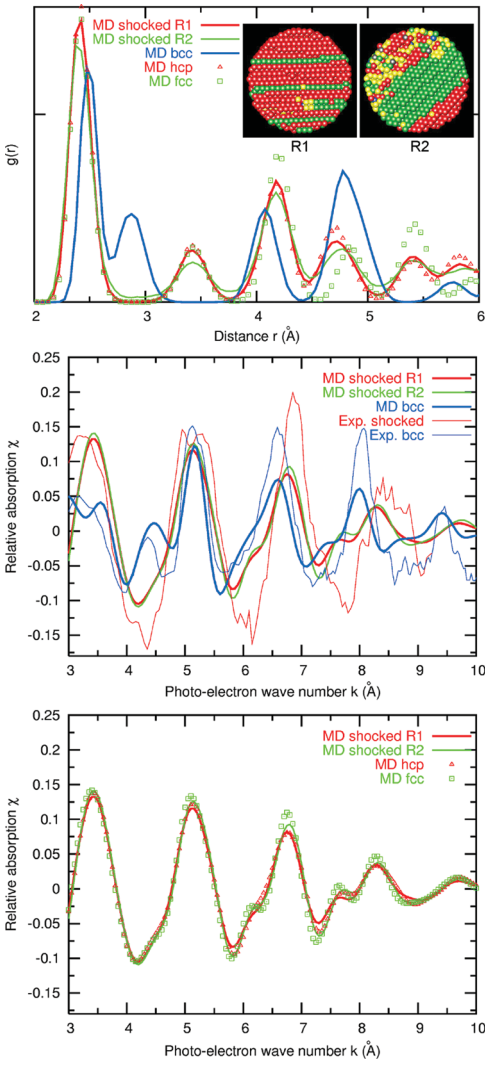

FIG. 3 (color). Radial distribution functions and EXAFS signal of several different cutouts (each containing about 5000 atoms) from the sample shown in Fig. 1 (bottom): purely bcc, region R1 (hcp/fcc ratio 3.2) and R2 (hcp/fcc ratio 1.03). The radial distribution and the EXAFS signals of the regions R1 and R2 are compared to ideal hcp and fcc structures simulated under the same pressure and temperature conditions. A comparison to experimental *in situ* EXAFS data [6] is shown in the middle panel.

300 K bcc EXAFS signal looks not as distinct as the experimental counterpart. However, the shocked state lies well above the Debye temperature and should not be affected that much by the classical distribution of phonons. Of course, the approximation of the interatomic force, as well as particularities of the experimental setup, can also lead to differences.

The present simulations of shock waves in polycrystalline iron demonstrate how atomistic modeling can enhance our understanding of ultrafast dynamical processes that take place in shock-induced phase transformations. Interpretations of experimental data can be scrutinized and checked with the simulation data set. Specifically,

atomistically simulated and experimental EXAFS spectra both support the conclusion that a phase transformation polycrystalline iron takes place under shock loading, yielding an almost isotropic close-packed product phase. However, the simulations also reveal the possibility of the product having some sizable fraction of metastable fcc product, as opposed to purely hcp. This question cannot be resolved from the experimental EXAFS spectra alone, since the noise levels for those ultrafast *in situ* measurements are too large to differentiate between hcp and fcc. We have to emphasize that details of the interatomic potential change the hcp to fcc ratio in the simulations [16]. However, all tested EAM potentials for iron [12,26] show a sizable fraction of fcc in the product phase under shock loading. Since the hcp/fcc ratio within a grain decreases the more the shock direction deviates from the $[001]_{bcc}$ direction with respect to the initial polycrystal, a geometric component to this effect is speculated: The *ABC* stacking sequence along $[111]_{bcc}$ makes it easier to transform under rapid compression in this direction into the *ABC* stacked fcc structure instead of the *AB* stacked hcp phase. For shocks along $[001]_{bcc}$ the *AB* stacked close-packed bcc planes transforming into the *AB* stacked close-packed hcp planes more easily than into the *ABC* stacked fcc planes. Fully resolved *ab initio* MD simulations would allow for a more reliable predication of the hcp to fcc ratio of the product phase. However, such methods are presently far too computationally intensive for the large scales needed for a polycrystalline system. Our NEMD simulations were on the order of some 10 ps, still too short to detect further relaxation processes that might occur on longer time scales. We leave the final clarification of the detailed structure and relaxation of the product phase to planned high-energy laser-based experiments that can access time scales on the order of nanoseconds [4].

We would like to thank J. Barber (Los Alamos), J. Hawreliak (Livermore), E. M. Kober (Los Alamos), R. J. Ravelo (Texas-El Paso/Los Alamos), J. J. Rehr (Washington), J. Roth (Stuttgart), and B. Yaakobi (Rochester) for many fruitful discussions. This work was carried out under the auspices of the National Nuclear Security Administration of the U.S. Department of Energy at Los Alamos National Laboratory under Contract No. DE-AC52-06NA25396, with funding by ASC and No. LDRD-20050107DR. High-performance computer access through the Institutional Computing Program is gratefully acknowledged.

*Electronic address: kkadau@lanl.gov
†Electronic address: tcg@lanl.gov
‡Electronic address: pxl@lanl.gov
§Electronic address: rca@lanl.gov
‖Electronic address: justin.wark@physics.ox.ac.uk
¶Electronic address: andrew.higginbotham@physics.ox.ac.uk
**Electronic address: blh@lanl.gov

[1] D. Bancroft, E. L. Peterson, and S. Minshall, J. Appl. Phys. **27**, 291 (1956).
[2] J. C. Jamieson and A. W. Lawson, J. Appl. Phys. **33**, 776 (1962).
[3] K. Kadau, T. C. Germann, P. S. Lomdahl, and B. L. Holian, Science **296**, 1681 (2002).
[4] D. H. Kalantar *et al.*, Phys. Rev. Lett. **95**, 075502 (2005).
[5] K. Kadau, T. C. Germann, P. S. Lomdahl, and B. L. Holian, Phys. Rev. B **72**, 064120 (2005).
[6] B. Yaakobi, T. R. Boehly, D. D. Meyerhofer, T. J. B. Collins, B. A. Remington, P. G. Allen, S. M. Pollaine, H. E. Lorenzana, and J. H. Eggert, Phys. Rev. Lett. **95**, 075501 (2005).
[7] P. S. Lomdahl, P. Tamayo, N. G. Jensen, and D. M. Beazley, in *Proceedings of Supercomputing '93*, edited by G. S. Ansell (IEEE Computer Society Press, Los Alamitos, CA, 1993), p. 520.
[8] D. M. Beazley and P. S. Lomdahl, Comput. Phys. **11**, 230 (1997).
[9] K. Kadau, T. C. Germann, and P. S. Lomdahl, Int. J. Mod. Phys. C **15**, 193 (2004).
[10] M. S. Daw and M. I. Baskes, Phys. Rev. Lett. **50**, 1285 (1983).
[11] M. S. Daw and M. I. Baskes, Phys. Rev. B **29**, 6443 (1984).
[12] R. Harrison, A. F. Voter, and S.-P. Chen, in *Atomistic Simulation of Materials*, edited by V. Vitek and D. J. Srolovitz (Plenum Press, New York, 1989), p. 219.
[13] A. Belonoshko and R. Ahuja, Phys. Earth Planet. Inter. **102**, 171 (1997).
[14] A. Okabe, B. Boots, and K. Sugihara, *Concepts and Applications of Voronoi Diagrams* (Wiley, Chichester, 1992).
[15] B. L. Holian and P. S. Lomdahl, Science **280**, 2085 (1998).
[16] See EPAPS Document No. E-PRLTAO-98-019712 for movies of simulations, additional pictures, and radial distributions illustrating the structure of polycrystalline iron after shock passage for various shock strengths and grain sizes. For more information on EPAPS, see http://www.aip.org/pubservs/epaps.html.
[17] T. de Resseguier and M. Hallouin, J. Appl. Phys. **84**, 1932 (1998).
[18] B. J. Jensen, P. A. Rigg, M. D. Knudsen, R. S. Hixson, G. T. Gray, III, B. C. Sencer, and F. J. Cherne, AIP Conf. Proc. **845**, 232 (2006).
[19] J. M. Brown, J. N. Fritz, and R. S. Hixson, J. Appl. Phys. **88**, 5496 (2000).
[20] R. G. McQueen, S. P. Marsh, J. W. Taylor, J. N. Fritz, and W. J. Carter, in *High-Velocity Impact Phenomena*, edited by R. Kinslow (Academic, New York, 1970), pp. 293–417.
[21] T. C. Germann, B. L. Holian, P. S. Lomdahl, and R. Ravelo, Phys. Rev. Lett. **84**, 5351 (2000).
[22] M. A. Meyers and M. S. Carvalho, Mater. Sci. Eng. **24**, 131 (1976).
[23] E. M. Bringa, A. Caro, M. Victoria, and N. Park, JOM **57**, 67 (2005).
[24] C. L. Kelchner, S. J. Plimpton, and J. C. Hamilton, Phys. Rev. B **58**, 11085 (1998).
[25] J. J. Rehr, R. C. Albers, and S. I. Zabinsky, Phys. Rev. Lett. **69**, 3397 (1992).
[26] R. Meyer and P. Entel, Phys. Rev. B **57**, 5140 (1998).